Applied Catalysis B: Environmental 232 (2018) 155–163

Contents lists available at ScienceDirect

Applied Catalysis B: Environmental

journal homepage: www.elsevier.com/locate/apcatb

Continuous esterification of oleic acid to ethyl oleate under sub/supercritical conditions over γ-Al_2O_3

Jiuxu Liu, Yue Nan, Xinlei Huang, Jesse Q. Bond, Lawrence L. Tavlarides*

Department of Biomedical and Chemical Engineering, Syracuse University, 329 Link Hall, Syracuse, NY, 13244, United States

ARTICLE INFO

Keywords:
Esterification
Oleic acid
Subcritical and supercritical conditions
γ-Al_2O_3

ABSTRACT

Esterification of oleic acid with ethanol was conducted under subcritical and supercritical conditions in a packed-bed reactor containing γ-Al_2O_3. The presence of γ-Al_2O_3 significantly improved the reaction rate such that the 42% yield achieved at 325 °C, 200 bar, and 1-min residence time without the alumina was increased to 98% at the same conditions when alumina was present. The catalytic capacity was attributed to Lewis acid sites on the surface of alumina, and non Brønsted acid sites were detected. Experiments to study the kinetics were executed at a pressure of 200 bar, elevated temperatures (200, 225, 275, 300, and 325 °C), and residence times of half to 8 minutes. Mass transfer limitations were estimated to be negligible via the Mears and Weisz-Prater criteria. Kinetic analysis based on the one-step model demonstrates that the overall reaction was endothermic, and an Eley-Rideal (ER) reaction mechanism was proposed to describe each elementary reaction step. The stability of γ-Al_2O_3 on product conversion was tested via a 25 h operation under 325 °C, 200 bar, and 1 min residence time, and decrease of the conversion was not observed. However, results of the catalyst analytical characterization shows a decrease of the acid site density and surface area, supporting the occurrence of catalyst degradation. The addition of water slightly decreased the yield, while the pressure change from 200 to 100 bar did not have an obvious effect on the conversion.

1. Introduction

Considerable amounts of wastewater is generated in biodiesel industry in order to remove the dissolved homogeneous catalysts from the product [1,2]. Plus, the production cost of biodiesel is expensive, since current industry uses refined oils including soybean, palm, and rapeseed oil as the feed stocks considering that the homogeneous catalysts are sensitive to the presence of free fatty acids and water which are present in cheap low-quality oils [3]. These problems could be solved via subcritical and supercritical reaction conditions (SC). The SC conditions are created by increasing the reaction temperature and pressure to values near or above the critical point of the alcohol. Under such severe conditions, the properties of alcohol are changed such as density of hydrogen bonding in alcohols significantly decreases, and alcohols become nearly non-polar [4,5,6]. These changes contribute to the mixing of alcohols and oils to have the reactions performed in a homogeneous reaction phase which minimizes mass transfer resistance and therefore significantly increases the reaction rate. The high reaction temperatures also benefit the reaction rate. Due to the fast reaction rate under SC conditions, it is possible to perform the reactions non-catalytically, which eliminate the contamination problem as mentioned above. Additionally, the SC method could be more economically competitive compared to current industrial technology [7,8], since it can directly use low-quality and low-cost oils and hydrous alcohols [9–11].

However, biodiesel fuel will be thermally decomposed when temperatures exceed 350 °C [12,13], which further degrades fuel qualities [14–16]. In order to complete the SC reactions at temperatures lower than 350 °C in short reaction times to avoid decomposition reactions, one can add catalysts into the SC reaction media. Some researchers showed that a near complete yield was reached at 225 °C, 200 bar and 5 minutes by adding trace amount of strong basic homogeneous catalysts [17]. Stable heterogeneous (solid) catalysts are also expected to provide a similar product yield under SC conditions.

Solid catalysts can be acidic or basic. The popular basic catalysts include hydroxides, dolomites, hydrotalcites, mixed basic metal oxides, loaded and supported alkaline elements and oxides, which are commonly used under conventional conditions in biodiesel synthesis. In specific, CaO-based compounds including pure CaO [18] and loaded CaO [19,20], and potassium-based compounds including loaded KF [21], KI [22], and KOH [22] have drawn numerous attention due to their high activity and wide availability. Other alkaline metal oxides such as MgO [23], ZnO [24] and SrO [24] have also been studied by

* Corresponding author.
E-mail addresses: jliu23@syr.edu (J. Liu), lltavlar@syr.edu (L.L. Tavlarides).

https://doi.org/10.1016/j.apcatb.2018.03.050
Received 18 November 2017; Received in revised form 9 March 2018; Accepted 16 March 2018
Available online 19 March 2018
0926-3373/ © 2018 Elsevier B.V. All rights reserved.

different researchers. Even though high product yields were reached by applying these basic catalysts, serious leaching problems were found and the active compounds were detected in biodiesel product with high concentrations even at mild conditions. The acidic catalysts to synthesize biodiesel include acidic metal oxides [25], sulfated/ tungstated metal oxides [26–30], sulfonic ion-exchange resin, heteropolyacids, zeolites, and etc. Since the catalytic capacity of the acidic solids is lower than solid bases, the reactions with the acids were executed under more severe conditions. Similarly, most of the acidic solids were not stable under the reaction conditions due to leaching and other issues, despite high yields were achieved initially.

A literature review indicates that several synthesized compounds were found to be relatively stable even at temperatures higher than 190 °C including Zr-SBA-15 [31], $ZnAl_2O_4$ [32], and ZnO–TiO_2–Nd_2O_3/ZrO_2 [33]. Zr-SBA-15 (mixture of zirconia and mesoporous silica) was tested by Melero et al. [31] in a packed-bed reactor at 210 °C, 70 bar, and residence time of 30 min for which the reaction yield reached 96% with negligible catalyst leaching. Biodiesel yield of 70% was obtained at 210 °C and 4 h reaction time in a batch reactor containing $ZnAl_2O_4$ reported by Pugnet et al. [32]. Zinc leaching was very low that no more than 4 ppm by weight was detected in the ester phase after 6 h of contact time. By conducting the reactions in a packed-bed reactor over ZnO-TiO_2-Nd_2O_3/ZrO_2 at 200 °C and 69 min residence time, 95% biodiesel yield was reported by Kim et al. [33], and the leaching of ZnO was determined to be negligible by ICP analysis.

Some simple and largely available metal oxides such as titania, zirconia and alumina have been commonly used as catalyst supports due to their thermal and mechanical stability even at SC conditions. However, they did not show any catalytic ability under conventional conditions (T = 70 °C, ambient pressure) due to their weak acidic properties. McNeff et al. [34] reported that under SC conditions, reactions with alumina, zirconia, and titania, reached conversions over 90% at 360 °C and 200 bar. However, the temperatures proposed were too severe, which degraded biodiesel. Due to the very limited information, the optimal SC conditions for biodiesel production over the simple metal oxides are still unknown.

Generally speaking, information regarding synthesizing biodiesel fuel under SC conditions with heterogeneous catalysts is very limited. Besides, kinetics of the alcoholysis with heterogeneous catalysts under SC conditions are rarely reported in the literature, although kinetic studies for biodiesel production at conventional conditions with heterogeneous catalysts have received much attention over the past few decades [35–44].

Accordingly, this study aims to (1) explore the possibility of converting free fatty acids, which largely exist in waste cooking oils and animal tallows, to biodiesel fuel under SC conditions at short residence times over alumina powder, and (2) to study the kinetics for the catalytic reaction systems, neither of which is well addressed in the literature. The reactions were performed in a packed-bed reactor containing γ-Al_2O_3 under SC conditions (temperature from 200 to 325 °C, and pressure from 100 to 200 bar). Oleic acid was employed to represent all free fatty acids that could exist in cheap oils. Although methanol is preferred in biodiesel industry considering its cheaper cost, in this study ethanol was chosen as the alcohol instead of methanol, since ethanol has a better solubility with oleic acid than methanol. The improved solubility will benefit the mixing of reactants and minimize the mass transfer resistance. The reactions of methanol-based biodiesel synthesis should share the same mechanism of ethanol-based biodiesel due to the similar chemical and physical properties of the two alcohols.

2. Experimental

2.1. Material

Anhydrous ethanol (200 proof, 100 vol%) was purchased from Pharmco-Aaper. Oleic acid, GC analytical standards for oleic acid and ethyl linoleate, white quartz (50 + 70 mesh), *n*-methyl-*n*-(trimethylsilyl) trifluoroacetamide (MSTFA) (GC derivatization synthesis grade), and pyridine were purchased from Sigma Aldrich. *n-Heptane* (HPLC grade) was provided by Thermo Fisher Scientific. Deactivated glass wool used in reactor packing was purchased from Restek Corporation. Gases (ultrahigh purity grade) used in GC, FTIR, and TPD analysis were supplied by Airgas. γ-Al_2O_3 was provided by Acros in neutral form.

2.2. Catalyst characterization

The fresh catalyst were tested at 150 °C under vacuum for 10 h, and it was found negligible mass change. This suggests high purity of the catalyst, and the moisture and other deposit on the fresh catalyst was negligible. Accordingly, no further treatment was applied, and the fresh catalyst was directly used in the esterification reactions.

Powder XRD investigation was performed using a Bruker D8 Advance ECO powder diffractometer with Cu Kα radiation (λ = 0.154 nm) at 40 kV and 25 mA with a step size of 0.02 in the 2θ angle range of 15–70°.

Scanning electron microscope (JEOL) was utilized to physically observe the morphology of the fresh and spent catalyst.

N_2 adsorption-desorption isotherms were conducted by Micromeritics ASAP 2020 (adsorption of N_2 at 77 K). Prior to N_2 dosing, samples were degassed under vacuum (423 K, 8 h). Brunauer-Emmett-Teller (BET) and t-plot analyses were used to determine total and micropore surface areas. Barrett-Joyner-Halenda (BJH) analysis of the adsorption branch of N_2 isotherms was used to determine pore size distributions and average pore diameters. Pore volumes were calculated from cumulative nitrogen uptake at a relative pressure of 0.99.

Density of Lewis acid sites was determined from temperature programmed desorption (TPD) of ammonia [45]. Typically, approximately 70 mg of sample was inserted into a 1/2 inch quartz tube between two quartz wool (Grace) end plugs and the whole tube was further placed in an Omega furnace. The temperature of the furnace was regulated by a process controller (Love, series 16 A) and monitored by a type K thermocouple (Omega). All samples were calcined (4 h, 723 K, 3 K/min) under air flow (50 scm^3/min) before analysis. After cooling to 423 K, samples were purged in dry He flow (100 scm^3/min) for more than 90 min. Catalysts were further dosed with ammonia (1% ammonia and 1% argon, Airgas) flow. After saturation of ammonia on the surface, physically adsorbed ammonia was removed by applying a high He flowrate (400 scm^3/min) for at least 1 h. The furnace was then ramped to 973 K (10 K/min) under He including 1% Ar serving as an internal standard. Chemisorbed ammonia was removed after ramping. During the whole process, a mass-selective residual gas detector (Stanford Instruments RGA 100) was used to track MS signals of ammonia (m/z = 16) and Ar (m/z = 40) in the effluent.

Brønsted acid sites to Lewis acid sites ratio was determined using pyridine FTIR (Nicolet 6700 DTGS detector). 15–25 mg of catalysts were pressed into a 13 mm pellet through a hydraulic press. The pellet was loaded on an in-situ cell, designed and built in house. Samples were calcined as the procedure described before. Subsequently, the cell was cooled to 423 K, and purged under a flow of 60 scm^3/min of He gas. The He was purified by a liquid nitrogen trap followed by a moisture trap. The pellet was then dosed with 4 torr of pyridine (Sigma Aldrich, 99%). After the pellet was fully saturated, the cell was purged under a He flow of 200 scm^3/min at 423 K to remove physically adsorbed pyridine. Spectra were collected at 423 K. and Brønsted to Lewis ratios were determined by the ratio of the integrated IR bands at 1545 cm^{-1} (pyridimium ion) and 1455 cm^{-1} (pyridine) respectively, by applying the appropriate molar extinction coefficients [46] However, the prime quantities of interest in this study are Lewis site densities since no Brønsted acid sites was detected. The operation procedures for FTIR and TPD can be also found as described in prior publications, respectively [47,48].

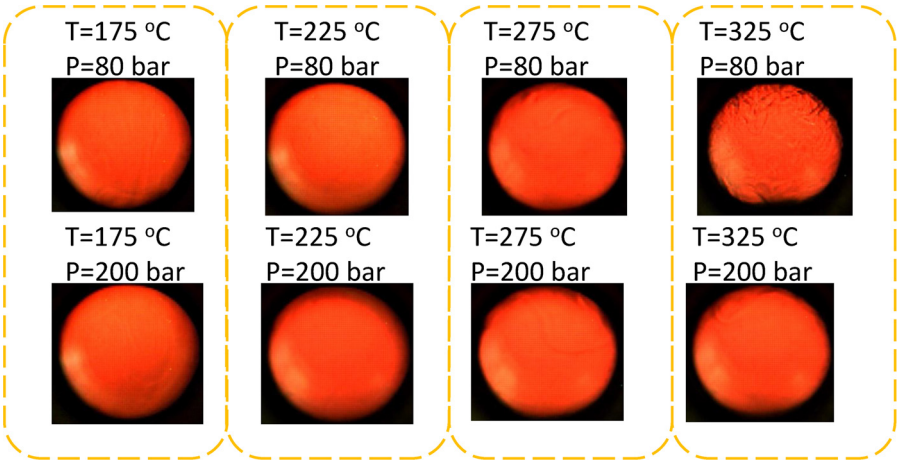

Fig. 1. Mixtures of ethanol-oleic acid (EtOH/OA molar ratio of 18) flowing through a view cell (V ~1 ml) at various conditions (T = 175–325 °C, P = 80–200 bar). The flow rates of the mixture were the same as which created one min residence time in the reactor in the reaction experiments.

2.3. Esterification reactions under SC conditions

Esterification reactions of oleic acid with ethanol (T_c = 241 °C, P_c = 63 bar) were executed in a downflow tubular reactor (316SS, ID 4.57 mm*25 cm). The γ-Al_2O_3 catalyst bed was held in place by two deactivated quartz wool plugs. The quartz wool was determined to have no activity, and it was widely used in reactor packing and TPD glass column packing [49,50]. The tube upstream and downstream of the catalyst bed was packed with white quartz to minimize dead volume.

Temperature (200–325 °C), pressure of 200 bar, and ethanol-to-oleic acid molar ratio of 18:1 were employed to perform experiments for the kinetics study. For temperature at 325 °C, pressures ranging from 100 to 200 bar were applied to investigate the pressure effect. The reaction residence time ranged from half to ten minutes. During experiments, oleic acid and ethanol were pressurized and transported using high pressure syringe pumps (Teledyne ISCO 260 D), preheated by heating tapes, mixed by passing through a mixing tee, and flowed into the reactor which was heated by an electrical furnace (Briskheat). The entire experimental set-up for conducting the reactions was similar as employed in our previous study, except for the reactor, including high-pressure syringe pumps, furnace, temperature controllers, thermocouples, back-pressure regulator, and data acquisition system [51]. The experimental errors were determined within 5% by performing duplicated runs, which demonstrates a stable reaction system. Collected samples were washed with distilled water before GC analysis to remove the dissolved ethanol.

Desired residence time was reached by precisely controlling pump flow rates, and it was defined as

$$\tau = \frac{VB \cdot \varepsilon}{FE \cdot (\rho E/\rho' E) + FO \cdot (\rho O/\rho' O)} \quad (1)$$

where V_B is volume of the empty-bed reactor, ε is the fraction of void to bed volume and it was experimentally determined by immersing the catalytic bed in ethanol. F is volumetric flow rate provided by the pumps, ρ is density of the oleic acid and ethanol (pump temperature, pump pressure), ρ' is density of the oleic acid and ethanol at reaction conditions, whose values are determined from the literature [52]. E and O represent ethanol and oleic acid, respectively.

The mixing of ethanol-oleic acid streams before reaching the packed-bed was physically observed through a view-cell system which consists of high pressure pumps (Teledyne ISCO 260 D), high pressure view-cell, a charge-coupled-device (CCD) camera with a micro-lens (Photron, model# FASTCAM-512PCI), light source, and data acquisition system. This experimental setup was also used in our previous study [51].

2.4. Biodiesel sample analysis

For the analysis of the FAEE profile, biodiesel samples were prepared by diluting 4 µl biodiesel into 1 ml heptane, making a total biodiesel concentration of 4000 ppm by volume. The samples were derivatized using MSTFA based on procedures provided in ASTM D6584 [53]. Quantitative analysis to measure the concentration of FAEE and oleic acid was conducted via a GC FID (HP 5890 Series II) equipped with an autosampler (HP 5890 Series II) and a DB-WAX column (30 m × 0.32 mmID × 0.50 µm, Restek) at splitless mode. Calibration curves for each compound were prepared by diluting the GC standards. The temperature program was as follows: held at 60 °C for 2 min, ramp at 6 °C/min from 60 °C to 240 °C, and held at 240 °C for 30 min. Concentrations of ethanol and water were determined from mass balance calculations since the initial concentration of ethanol and oleic acid were known (MR of 18:1) and the concentration of oleic acid and FAEE in the collected samples were measured from GC FID analyses. The yield of biodiesel is defined as the ratio of the true biodiesel content in a sample to the maximum biodiesel content assuming all oleic acid was converted to biodiesel.

ICP Mass 6100 Spectrometer was employed to test aluminum concentration in some biodiesel samples. It was found that the aluminum concentration was in ppb level which was very comparable to the blank.

3. Results and discussion

3.1. Mixing of ethanol-oleic acid streams

Mixing phenomena of ethanol-oil streams was studied during the heating and pressurizing process via a view-cell experimental setup in order to determine the significance of mass transfer resistance on conversion. Selected results are reported in Fig. 1. It is known that at ambient conditions, ethanol is only partially miscible with oleic acid. Elevating the temperatures (175–325 °C) and pressure (80–200 bar), the ethanol-oleic acid mixtures formed a homogeneous state, which indicates that at the selected reaction conditions (T: 200-325 °C, P: 100–200 bar) the reaction streams formed a homogeneous phase before contacting with the packed-bed, and accordingly mass transfer resistance between ethanol and oleic acid boundaries could not be significant.

3.2. Preliminary investigation on esterification of oleic acid over γ-Al_2O_3

Preliminary experiments using γ-Al_2O_3 were executed and compared with non-catalytic reactions in order to determine if the weak

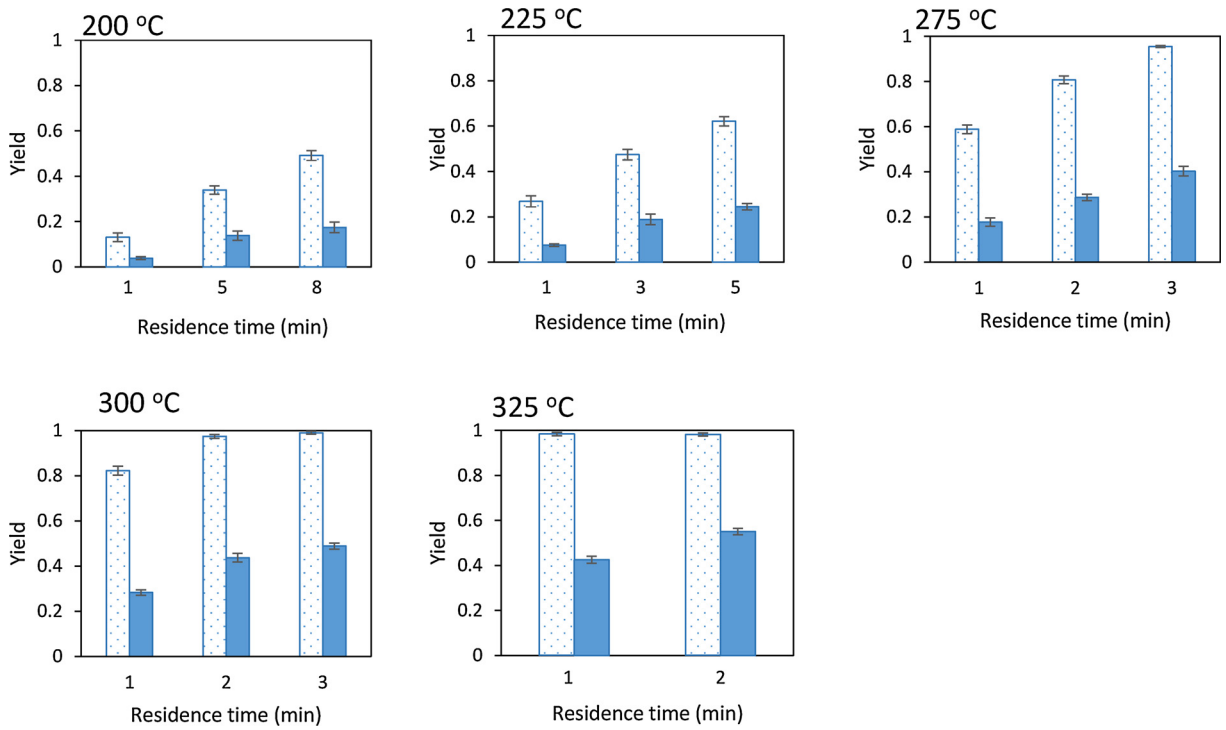

Fig. 2. Comparison of biodiesel yield of the reaction catalyzed by alumina (□) with the one without any catalysts (■). The reaction pressure was fixed at 200 bar.

solid acid would perform well in this reaction system. As shown in Fig. 2, at temperature of 200 °C, pressure of 200 bar, and residence time of 8 min, the yield for non-catalytic reactions was only 17%, while the yield was increased to 49% when γ-Al_2O_3 was employed. Similarly, at temperature of 225 °C and residence time of 5 min, the yield was increased from 24% to 62% when switching from non-catalytic to γ-Al_2O_3. Due to the weak acid property of alumina, the yields of the esterification reaction were not satisfying under the subcritical conditions in short residence times. The performance of the alumina was significantly enhanced under supercritical conditions. At 275 °C and 200 bar, the reaction with alumina reached a yield of 95% in 3 min compared to a non-catalytic yield of 40% at same condition. At 300 °C and 2 min, the yield of alumina-catalyzed reaction was 98% compared to a yield of 48% for the non-catalytic reaction. Similarly, at 325 °C and 1 min, near complete yield was obtained with alumina while only 42% was reached by the non-catalytic reaction. The results above demonstrate a high catalytic capacity of γ-Al_2O_3 for the esterification reaction under supercritical conditions. No by-product was observed.

3.3. Kinetics of esterification of oleic acid over γ-Al2O3

The reaction mechanism of esterification over heterogeneous Lewis acid was well described in the literature [54]. Similarly, in this study the mechanism, *Eley-Rideal* (ER), of the esterification reaction taking place between oleic acid and ethanol over γ-Al_2O_3 is proposed here as shown in Fig. 3. The carbonyl group in oleic acid molecule is adsorbed on acidic site of the alumina surface which has positive formal charge. The interaction of the carbonyl oxygen of oleic acid with acidic site of the catalyst forms carbocation, which makes the adjoining carbon atom susceptible to nucleophilic attack. Then the oxygen atom in ethanol molecule attacks the carbocation to form a tetrahedral intermediate. Then the tetrahedral intermediate eliminates the water molecule via the esterification reaction to form one molecule of ethyl oleate. In the last step, the catalyst is regenerated by desorbing ethyl oleate from the Lewis acid site.

Data points in Fig. 4 illustrate the concentration profile of each compound including the original reactants, oleic acid (OA) and ethanol, and final products ethyl oleate (FAEE) and water produced at 275–325 °C with γ-Al_2O_3. As expected, concentration of OA and ethanol were decreasing along with reaction time, whereas that of FAEE and water increased over time. At the last stage of conducted reactions, the amount of OA was reduced to a negligible level under supercritical conditions, however significant amounts still remained under the subcritical reactions. Specifically, at 275 °C and 5 min, 300 °C and 3 min, and 325 °C and 1 min, most of OA was reacted providing yields over 98% as shown in Fig. 4. However, trace amount of OA was still detected at these temperatures even if the residence time was extended, which implies the esterification reaction was reversible and had reached equilibrium. Also, the temperature changing from 275 to 325 °C did not influence the final equilibrium significantly which indicates the reaction could be thermally neutral. Lower temperatures make the reactions perform with slower reaction rate. At 200 and 225 °C with a 8 min residence time, a yield of only about 49% and 79% was reached, respectively, as calculated from data in Fig. 5.

Theoretical analysis of transport limitations in the packed-bed reactor are discussed in supplementary material in details. Mears, as shown in Eq. (2), and Weisz–Prater, as shown in Eq. (3), criteria were employed to estimate the interphase mass transfer limitations and intraparticle diffusion limitations, respectively, both of which were determined to be negligible. For example, at conditions of temperature of 325 °C, pressure of 200 bar, and residence time of 1 min, the term on the left hand side of Eq. (2) was calculated as $7.75*10^{-5}$ satisfying the Mears criterion, and the term on the left hand side of Eq. (3) was determined as $2.72*10^{-3}$ satisfying the Weisz-Prater criterion.

$$\frac{-r_A \rho_b R n}{k_c C_{Ab}} < 0.15 \tag{2}$$

where $(-r)$ is the rate of the reaction per bed volume (kmol/kg cat/s), ρ_b is the bulk density of catalyst bed (kg/m^3), R is the average radius of catalyst particles (m), n is the order of the reaction; C_{Ab} is the bulk concentration of the reactant oleic acid (kmol/m^3), and k_c is the mass transfer coefficient (m/s). Also,

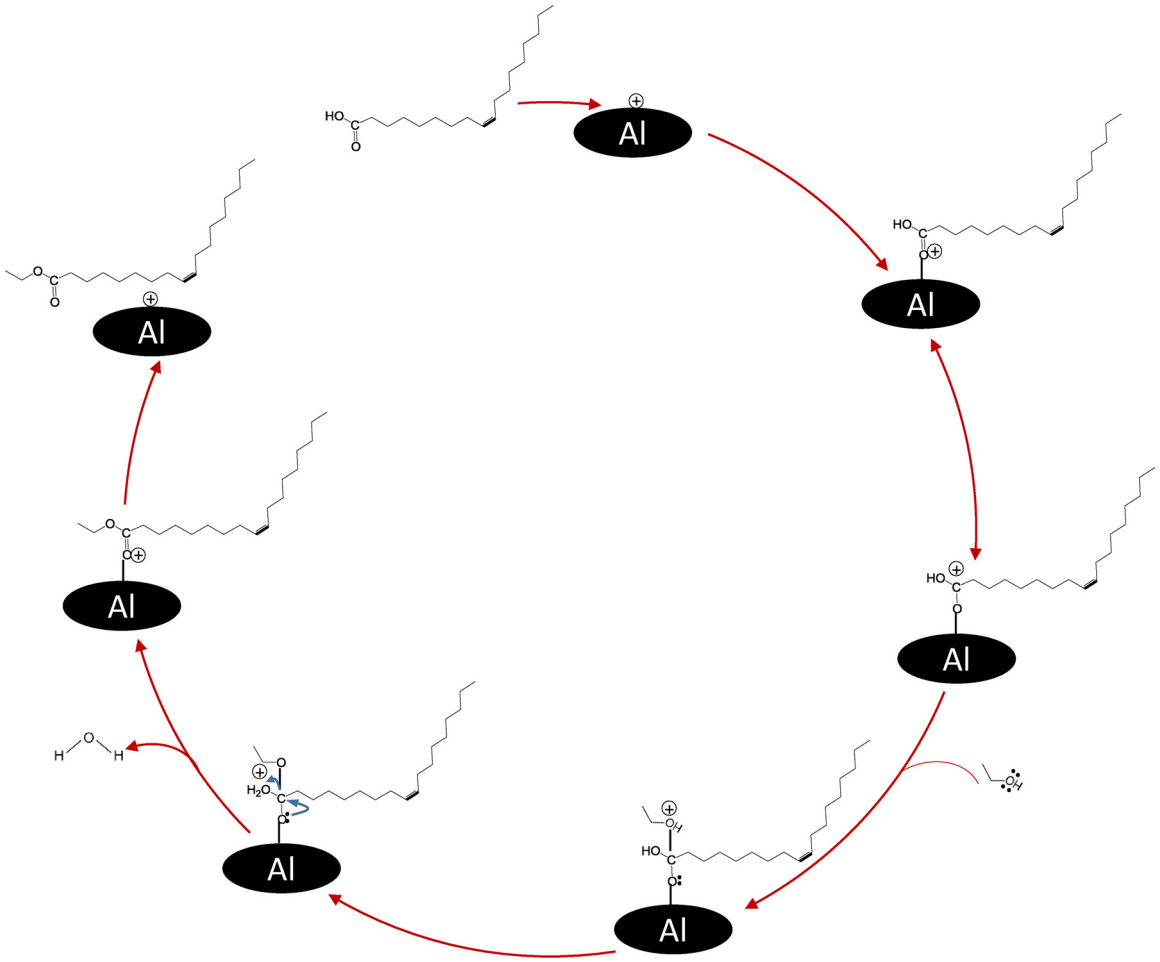

Fig. 3. Mechanism of esterification of oleic acid with ethanol over γ-alumina catalyst.

$$\frac{-r\rho_c R^2}{D_e C_{AS}} < 1 \quad (3)$$

where ρ_c is solid density of catalyst bed (kg/m^3), C_{AS} is the reactant concentration on alumina surface (kmol/m^3), and D_e is the effective diffusivity of oleic acid in methanol.

By neglecting the external and internal mass transfer resistances and assuming isothermal conditions and a steady state and 1D scenario, the pack-bed reactor model was simplified from Eq. (4) to Eq. (5).

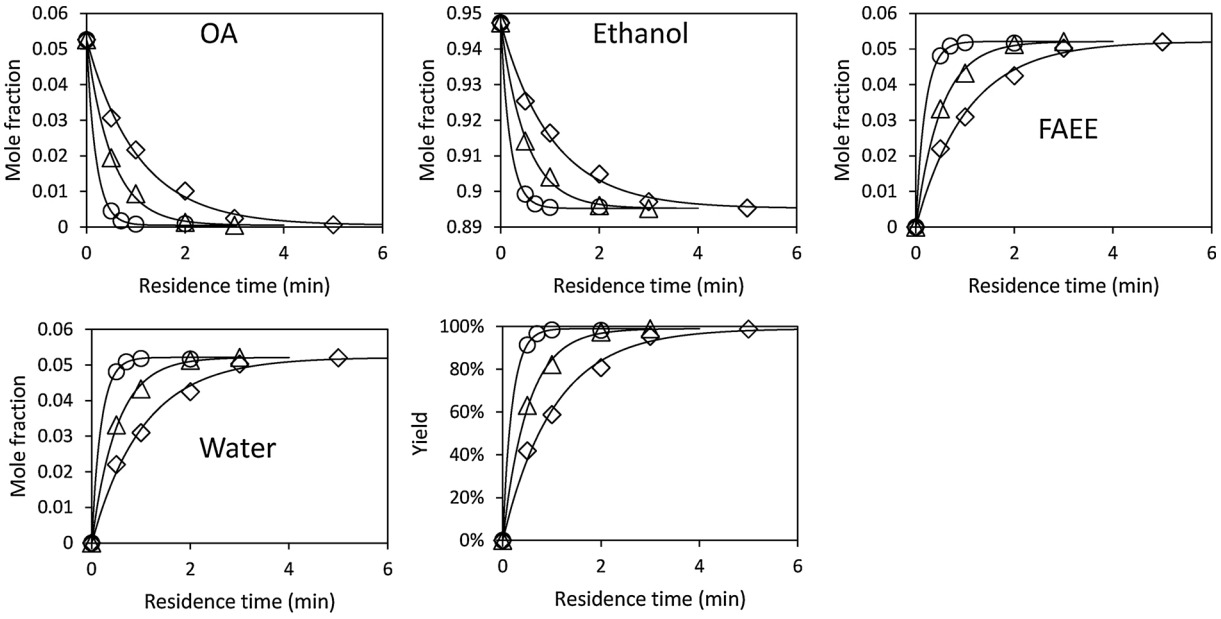

Fig. 4. Data fitting by the one-step classic model under supercritical conditions (T: 275–325 °C, P: 200 bar). Key: (◊) 275 °C, (Δ) 300 °C, (○) 325 °C.

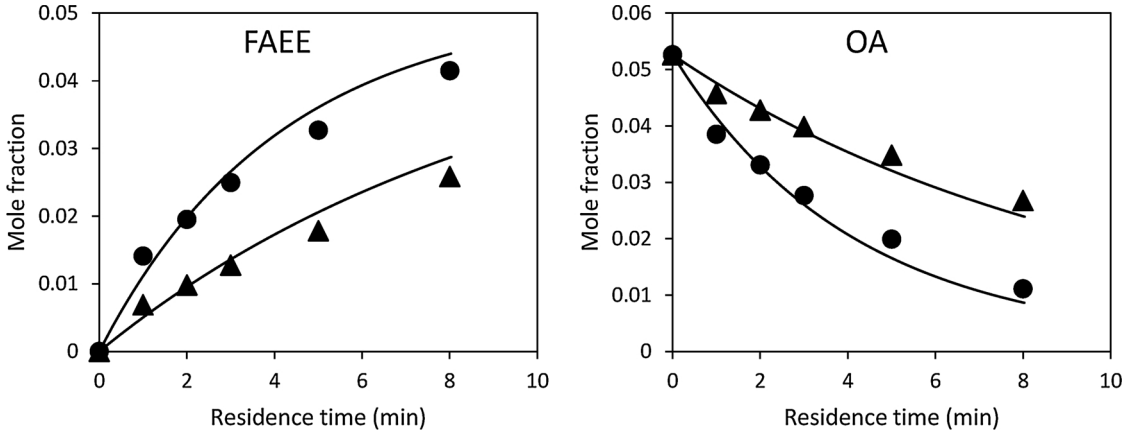

Fig. 5. Data fitting by the one-step classic model under subcritical conditions (T: 200–225 °C, P: 200 bar). Key: (▲) 200 °C, (●) 225 °C.

$$D_{AB}\left(\frac{\partial^2 C_A}{\partial x^2}+\frac{\partial^2 C_A}{\partial y^2}+\frac{\partial^2 C_A}{\partial z^2}\right)-U_x\frac{\partial C_A}{\partial x}-U_y\frac{\partial C_A}{\partial y}-U_z\frac{\partial C_A}{\partial z}+r=\frac{\partial C_A}{\partial t} \tag{4}$$

$$-U\frac{dC_{Ab}}{dz}+r=0 \tag{5}$$

In order to perform the macroscopic kinetic analysis of the esterification reaction, an one-step second-order reversible reaction model, as shown Eq. (6), was used to predict the global kinetic parameters and simulate the experimental data. Accordingly, the reaction rate can be expressed as Eq. (7).

$$OA + C_2H_5OH \underset{k_{-1}}{\overset{k_1}{\rightleftarrows}} FAEE + H_2O \tag{6}$$

$$r = k_1\left(C_{OA}\cdot C_{EtOH} - \frac{1}{K}C_{FAEE}\cdot C_{water}\right) \tag{7}$$

The simulation results for the supercritical reactions (T: 275–325 °C, P; 200 bar) are plotted in Fig. 4 as solid curves which show a good data fitting. The estimated k values are reported in Table 1 with the corresponding standard deviations. Then data of the subcritical reactions (T: 200 and 225 °C, P; 200 bar) are compared with ones predicted by the model where the k values were estimated by using the Arrhenius Equation which was determined by data of the supercritical reactions. The result is shown in Fig. 5, and it demonstrates a good predictability of the model.

The regressed values of *K*, the equilibrium constants, were plotted by the Van't Hoff equation, and the result shows a reasonable linearity with a R^2 of 0.98. Accordingly, the macroscopic reaction was experimentally found to be moderately endothermic ($\Delta H^\circ = 15.9\,kJ\,mol^{-1}$) and entropically favorable ($\Delta S^\circ = 39.3\,J\,mol^{-1}\,K^{-1}$). Qualitatively, these values are consistent with-albeit higher than analogous thermochemistry estimated from a simulated equilibrium

($\Delta H^\circ \approx 11\,kJ\,mol^{-1}$) [37]. The activation energy for the forward and reverse step is determined by applying the Arrhenius Equation as 74.9 and 58.9 kJ mol^{-1}, respectively.

Based on the *Eley-Rideal* (ER) reaction mechanism discussed above in Fig. 3, the elementary steps can be described as below. In this case, we consider that all adsorption and reaction steps involve a single type of active site, which is designated here as '*'. In this sequence, a molecule of oleic acid (OA) adsorbs at a Lewis site (*) on the surface as expressed in Eq. (8), then an ethanol molecule attacks the oleic acid to form one mole of ethyl oleate via esterification as written in Eq. (9). Finally, the catalyst is regenerated after desorbing ethyl oleate from the Lewis acid site as shown in Eq. (10). Accordingly, the equation of reaction rate can be expressed as in Eq. (11) if assuming the rate controlling step is the adsorption of oleic acid.

$$OA + * \overset{K1}{\rightleftarrows} OA* \tag{8}$$

$$OA* + C_2H_5OH \overset{K2}{\rightleftarrows} FAEE* + H_2O \tag{9}$$

$$FAEE* \overset{K3}{\rightleftarrows} FAEE + * \tag{10}$$

$$r = \frac{k_1 Ct\cdot\left(C_{OA} - \frac{C_{FAEE}C_{WATER}}{K_1K_2K_3C_{EtOH}}\right)}{1 + \frac{C_{FAEE}C_{WATER}}{K_2K_3C_{EtOH}} + \frac{C_{FAEE}}{K_3}} \tag{11}$$

The data were fitted to calculate the reaction rate and equilibrium constants at each step via least-squares regression. The results indicate a good fit in terms of R^2 values over 0.995. Unfortunately, considering that the total number of data points were relatively limited, wide confidence intervals for the regressed kinetic parameters including K_1, K_2, and K_3 were found when employing this complicated model, so we currently are not able to regress all set of the kinetic parameters from the experimental data to provide meaningful values. By conservative analysis using the Van't Hoff equation, the adsorption of oleic acid on the surface of alumina was estimated to be exothermic, the esterification and desorption of ethyl oleate from alumia were endothermic reactions. And the overall process in terms of a combination of the three elementary steps is endothermic based on the analysis from the one-step model.

Table 1
Estimated reaction rate constants for the one-step model.

	k_1 ± S.D.[a]	k_{-1} ± S.D.[a]
200 °C	0.089[b]	0.046[b]
225 °C	0.230[b]	0.093[b]
275 °C	1.015 ± 0.056	0.328 ± 0.237
300 °C	2.078 ± 0.035	0.526 ± 0.212
325 °C	5.554 ± 0.069	1.160 ± 0.109

[a] standard deviation.
[b] The values for 200 and 225 °C were estimated by using the Arrhenius Equation which was determined by the k values for 275–325 °C.

3.4. Stability of the alumina catalyst under supercritical conditions

In order to determine the stability of the alumina catalyst under supercritical conditions, the pack-bed was utilized to carry out the esterification reaction at 325 °C, 200 bar, and 1 min reaction time continuously for 25 h. Multiple biodiesel samples were collected and measured along with the process, and a decrease of the yield was not observed during this 25 h test. However, this does not prove the stability of the alumina catalyst, and it is very possible that there was more than enough catalyst in the reactor so the deactivation was not measurable even if it were occuring. Instead, the catalyst was taken out

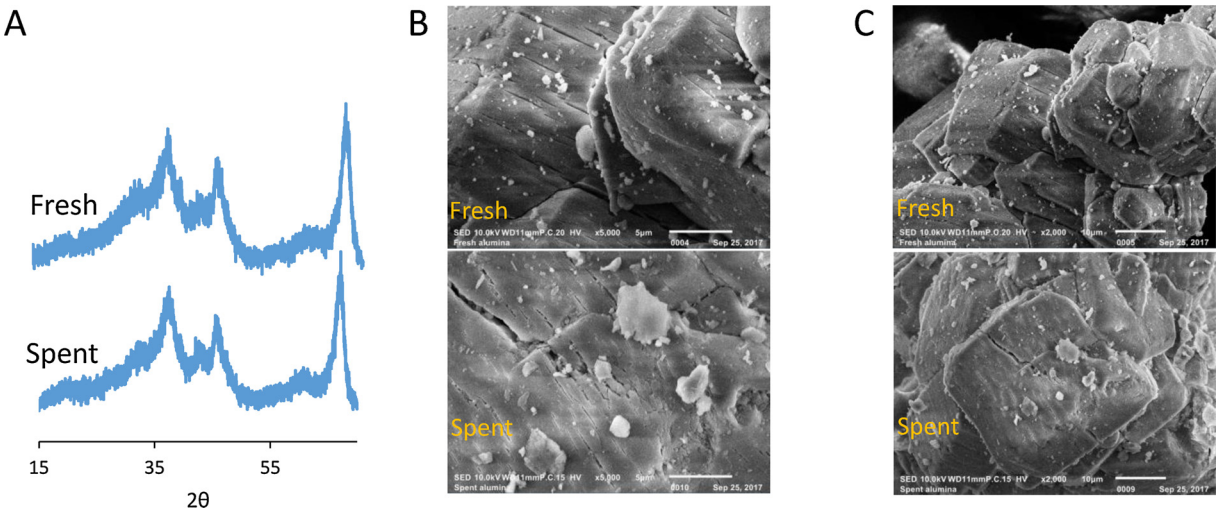

Fig. 6. (A) XRD analysis of the spent alumina catalyst before and after the stability test. Comparison of SEM analysis between fresh and spend alumina catalyst at magnification of (B) 5000 and (C) 2000.

from the reactor, and analyzed by different characterization tools as below.

The XRD analysis, as shown in Fig. 6A, tells that the fresh alumina was in gamma phase, and the spent alumina still remained in gamma phase, which demonstrates a stable crystal structure. In Fig. 6B and C, the morphology of the catalyst did not change obviously from observation by SEM analysis at different magnification.

However, data from BJH adsorption curve in Fig. 7A clearly show a decrease of pore distribution between 3 and 7 nm pore-diameter after being treated under the supercritical reaction. The BET surface area decreased from 126.7 to 99.2 m^2/g, and BJH pore volume changed from 0.24 to 0.19 cm^3/g after the continuous reaction, as shown in Table 2. By conducting the TPD analysis, the Lewis acid site density of the fresh alumina catalyst was estimated as 28.35 μmol/g which is comparable to the values shown in the literature [55]. The Lewis acid site density dropped from 28.35 to 17.15 μmol/g after the 25 h reaction, as also shown in Fig. 7B. Since the samples were calcined before TPD analysis as mentioned in the experimental section, the detected change of the active sites clearly demonstrates the deactivation of the catalyst. The cause could be carbon deposition, since we do observe the color of the alumina catalyst turned from white to gray. Similar thermal degradation of the alumina under sub/supercritical conditions were also observed in the literature [56]. The mechanism and kinetics of the alumina degradation will be included in future work by utilizing a differential reactor instead of a fully packed reactor.

Table 2
Comparison of physical properties of the alumina catalyst before and after the stability test.

	Lewis acid site density (μmol/g)	Brønsted acid site density (μmol/g)	BET surface area (m^2/g)	BJH adsorption pore volume (cm^3/g)
Fresh catalyst	28.35	0	126.72	0.24
Spent catalyst	17.15	0	99.16	0.19

3.5. Effect of water and pressure on the reactions

More than half cost of biodiesel fuel comes from refined oil and anhydrous alcohol costs which are required by the conventional biodiesel industry, since common impurities in the feedstocks of water and free fatty acids (FFA) deactivate the homogeneous catalysts as FFA react with base catalysts via saponification reactions, and water poisons both base and acid catalysts under conventional biodiesel synthesis conditions. However, it is not clear how these impurities would influence the supercritical reactions over the γ-Al_2O_3 catalyst. Usually water

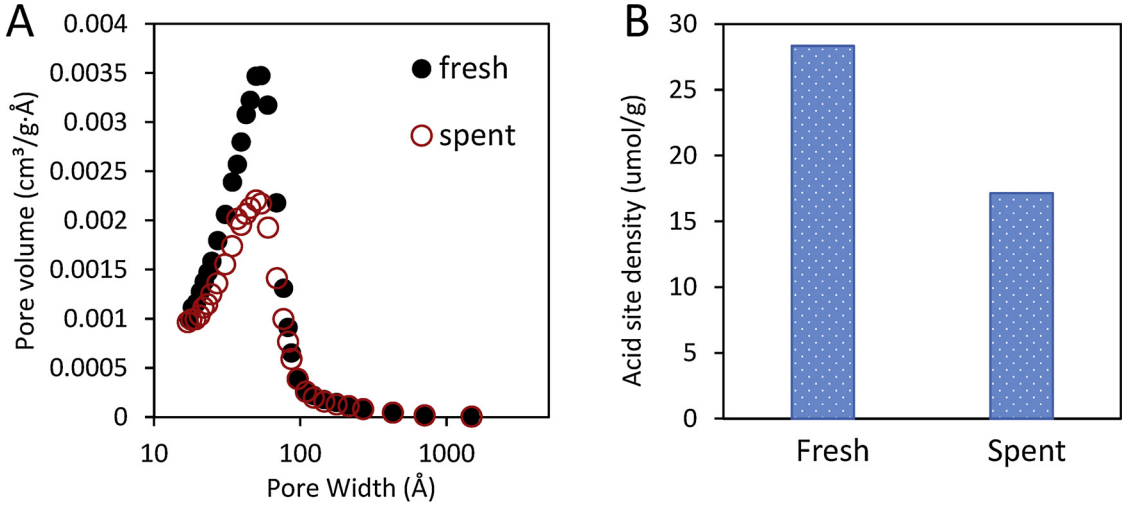

Fig. 7. Comparison of (A) BJH adsorption, and (B) Lewis acid sites density between fresh and spent catalyst.

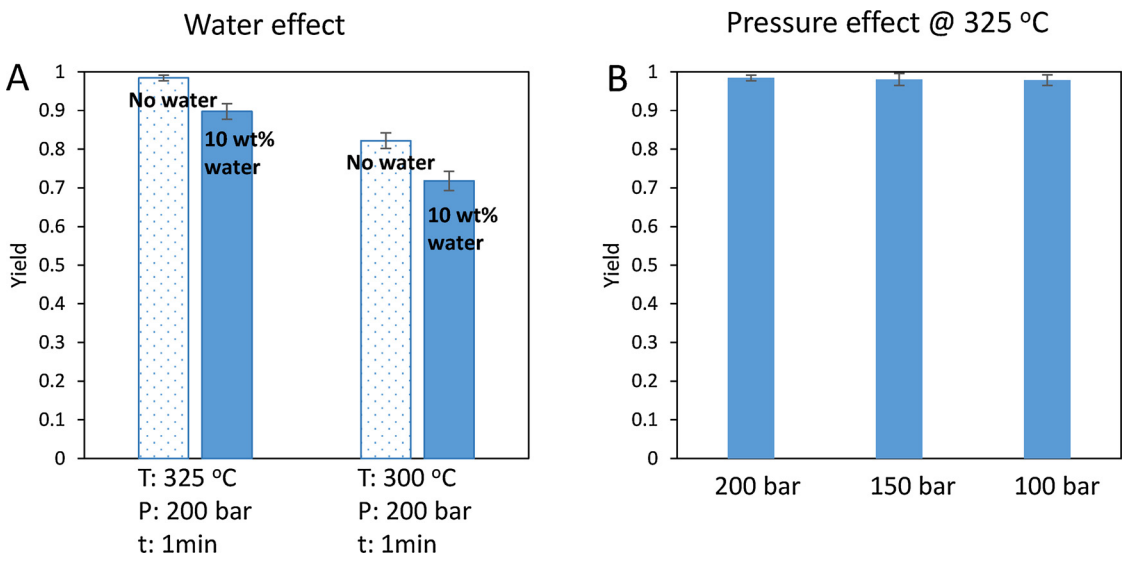

Fig. 8. Effect of impurities including water and pressure on product yield under SC conditions.

content in cheap feedstocks as waste cooking oil and hydrous ethanol before pretreatment exceeds 3 wt%. Accordingly, in this study, ethanol solution which contains 10 vol% water was used to study water effect on the reactions. As shown in Fig. 8A, when conducting reactions at temperature of 325 and 300 °C, pressure of 200 bar, and residence time of 1 minute, increasing water content in the ethanol from zero to 10 wt % results in the yield decrease from 99% to 90%, and from 84% to 72%, respectively. The decreasing yield could be due to the large presence of water which shifted the equilibrium to the left via hydrolyzing the FAEE to oleic acid, since water is one of the product besides FAEE, or that it turned the reaction phase less homogeneous which increased the mass transfer resistance of the reaction system. Also as reported in the literature, the alumina will be turned into a hydrated boehmite (AlOOH) phase, and the acidity and surface area will be decreased under treatment of sub/supercritical water conditions, which could also decrease the product yield [56]. Accordingly, water should be eliminated from the feedstock by pretreatment in order to prevent the yield from decreasing either from equilibrium shifting or alumina degradation by water.

High pressures of 200–300 bar are commonly used in studies related to sub/supercritical biodiesel synthesis in order to pressurize the reaction system into a homogeneous state. These required high pressures would bring potential safety issues and increase the cost of equipment. Adding co-solvent can improve solubilization of the alcohol-oil stream, but this also increases the product purification burden. In this study, pressure effect on reaction yield at supercritical conditions were investigated. As shown in Fig. 8B, at the stated conditions (T: 325 °C, t: 1 min, EtOH-Oil molar ratio: 18), the effect of pressure ranging from 100 to 200 bar on product yield was evaluated. The yield was monitored as nearly constant as 98%. The mixing of ethanol-oil stream was observed by the view-cell set-up, and it was found that in this pressure range the reaction mixture remained in a homogeneous state before contacting the packed-bed. This result demonstrates that the reaction yield will not be effected by pressure change as long as such change does not influence the reaction phase behavior. Experimental set-up such as a view-cell system and suitable equation of states can be employed to find minimum pressures experimentally and theoretically for specific conditions including temperature, alcohol-to-oil molar ratio, and flow rate, which can create a homogeneous reaction state.

4. Conclusions

The esterification of oleic acid with ethanol was carried out in a packed-bed reactor containing γ-Al_2O_3 catalyst under subcritical and supercritical conditions (T: 200–325 °C, P: 100–200 bar). The catalytic capacity of the alumina at supercritical conditions was considerably higher than at subcritical conditions, for example at pressure of 200 bar and one-minute residence time, about 99% yield was obtained at temperature of 325 °C and while only 27% yield was found at 225 °C. An one-step reaction model was used to well describe the data for the supercritical reactions, and it was capable of predicting the data for the subcritical reactions. The analysis demonstrates that the overall reaction including adsorption of oleic acid on the surface, the esterification reaction on the surface, and desorption of biodiesel from the surface is endothermic. Slowly deactivation of the catalyst was observed as a decreased acid site density and surface area, but the loss of product yield was not observed by the deactivation considering the large amount of catalysts employed. Large presence of water decreased the yield by around 10%, and dropping the pressure from 200 bar to 100 bar at 325 °C did not show obvious influence on the yield.

Acknowledgements

We are grateful to Syracuse University, College of Engineering and Computer Science for financial support. We thank Mr. Richard Louis List at SUNY ESF for his help on using the SEM. This work also made use of the Cornell Center for Materials Research Shared Facilities which are supported through the NSF MRSEC program (DMR-1719875).

Appendix A. Supplementary data

Supplementary material related to this article can be found, in the online version, at doi:https://doi.org/10.1016/j.apcatb.2018.03.050.

References

[1] C. Rattanapan, A. Sawain, T. Suksaroj, C. Suksaroj, Desalination 280 (2011) 370–377.
[2] D. Phukingngam, S. Dararat, O. Chavalparit, Bangkok, Thailand, Proceedings of the 7th National Environmental Conference (2008).
[3] L. Meher, D.V. Sagar, S. Naik, Renew. Sustain. Energy Rev. 10 (2006) 248–268.
[4] J. Lu, E.C. Boughner, C.L. Liotta, C.A. Eckert, Fluid Phase Equilib. 198 (2002) 37–49.
[5] P. Lalanne, J. Andanson, J. Soetens, T. Tassaing, Y. Danten, M. Besnard, J. Phys. Chem. A 108 (2004) 3902–3909.
[6] M.M. Hoffmann, M.S. Conradi, J. Phys. Chem. B 102 (1998) 263–271.
[7] A. Deshpande, G. Anitescu, P. Rice, L. Tavlarides, Bioresour. Technol. 101 (2010) 1834–1843.
[8] S. Lee, D. Posarac, N. Ellis, Chem. Eng. Res. Des. 89 (2011) 2626–2642.

[9] S.L. Gonzalez, M.M. Sychoski, H.J. Navarro-Díaz, N. Callejas, M. Saibene, I. Vieitez, I. Jachmanián, C. da Silva, H. Hense, J.V. Oliveira, Energy Fuels 27 (2013) 5253–5259.
[10] K.T. Tan, K.T. Lee, A.R. Mohamed, J. Supercrit. Fluids 53 (2010) 88–91.
[11] Y. Nan, J. Liu, R. Lin, L.L. Tavlarides, J. Supercrit. Fluids 97 (2015) 174–182.
[12] H. Shin, S. Lim, S. Bae, S.C. Oh, J. Anal. Appl. Pyrolysis. 92 (2011) 332–338.
[13] H. Imahara, E. Minami, S. Hari, S. Saka, Fuel 87 (2008) 1–6.
[14] R. Lin, Y. Zhu, L.L. Tavlarides, Fuel 117 (2014) 981–988.
[15] J. Liu, Y. Shen, Y. Nan, L.L. Tavlarides, Fuel 178 (2016) 23–36.
[16] R.O. Dunn, J. Am. Oil Chem. Soc. 79 (2002) 915–920.
[17] J. Liu, Y. Nan, L.L. Tavlarides, Fuel. 193 (2017) 187–196.
[18] I. Reyero, G. Arzamendi, L.M. Gandía, Chem. Eng. Res. Des. 92 (2014) 1519–1530.
[19] M. Zabeti, Wan Mohd Ashri Wan Daud, M.K. Aroua, Fuel Process Technol. 91 (2010) 243–248.
[20] C. Samart, C. Chaiya, P. Reubroycharoen, Energy Convers. Manage. 51 (2010) 1428–1431.
[21] Ž. Kesić, I. Lukić, D. Brkić, J. Rogan, M. Zdujić, H. Liu, D. Skala, Appl. Catal. A 427 (2012) 58–65.
[22] A. Islam, Y.H. Taufiq-Yap, P. Ravindra, S.H. Teo, S. Sivasangar, E. Chan, Energy 89 (2015) 965–973.
[23] M. Di Serio, M. Ledda, M. Cozzolino, G. Minutillo, R. Tesser, E. Santacesaria, Ind. Eng. Chem. Res. 45 (2006) 3009–3014.
[24] S.J. Yoo, H. Lee, B. Veriansyah, J. Kim, J. Kim, Y. Lee, Bioresour. Technol. 101 (2010) 8686–8689.
[25] J. Jitputti, B. Kitiyanan, P. Rangsunvigit, K. Bunyakiat, L. Attanatho, P. Jenvanitpanjakul, Chem. Eng. J. 116 (2006) 61–66.
[26] C.M. Garcia, S. Teixeira, L.L. Marciniuk, U. Schuchardt, Bioresour. Technol. 99 (2008) 6608–6613.
[27] S. Furuta, H. Matsuhashi, K. Arata, Catal. Commun. 5 (2004) 721–723.
[28] J. Kansedo, K.T. Lee, S. Bhatia, Biomass Bioenergy 33 (2009) 271–276.
[29] Y. Park, J.Y. Lee, S. Chung, I.S. Park, S. Lee, D. Kim, J. Lee, K. Lee, Bioresour. Technol. 101 (2010) S59–S61.
[30] B. Peng, Q. Shu, J. Wang, G. Wang, D. Wang, M. Han, Process Saf. Environ. Prot. 86 (2008) 441–447.
[31] J.A. Melero, L.F. Bautista, J. Iglesias, G. Morales, R. Sánchez-Vazquez, Appl. Catal. B: Environ. 145 (2014) 197–204.
[32] V. Pugnet, S. Maury, V. Coupard, A. Dandeu, A. Quoineaud, J. Bonneau, D. Tichit, Appl. Catal. A 374 (2010) 71–78.
[33] M. Kim, C. DiMaggio, S.O. Salley, K.S. Ng, Bioresour. Technol. 118 (2012) 37–42.
[34] C.V. McNeff, L.C. McNeff, B. Yan, D.T. Nowlan, M. Rasmussen, A.E. Gyberg, B.J. Krohn, R.L. Fedie, T.R. Hoye, Appl. Catal. A 343 (2008) 39–48.
[35] Y. Xiao, L. Gao, G. Xiao, B. Fu, L. Niu, Ind. Eng. Chem. Res. 51 (2012) 11860–11865.
[36] N.M. Ray, A.K. Ray, Can. J. Chem. Eng. 94 (2016) 738–744.
[37] R. Tesser, M. Di Serio, M. Guida, M. Nastasi, E. Santacesaria, Ind. Eng. Chem. Res. 44 (2005) 7978–7982.
[38] A. Kapil, K. Wilson, A.F. Lee, J. Sadhukhan, Ind. Eng. Chem. Res. 50 (2011) 4818–4830.
[39] F. Allain, J. Portha, E. Girot, L. Falk, A. Dandeu, V. Coupard, Chem. Eng. J. 283 (2016) 833–845.
[40] E. Santacesaria, R. Tesser, M. Di Serio, M. Guida, D. Gaetano, A. Garcia Agreda, Ind. Eng. Chem. Res. 46 (2007) 5113–5121.
[41] T.F. Dossin, M. Reyniers, R.J. Berger, G.B. Marin, Appl. Catal. B: Environ. 67 (2006) 136–148.
[42] H. Veny, M.K. Aroua, N.M.N. Sulaiman, Chem. Eng. J. 237 (2014) 123–130.
[43] B. Likozar, A. Pohar, J. Levec, Fuel Process Technol. 142 (2016) 326–336.
[44] Y. Xiao, L. Gao, G. Xiao, J. Lv, Energy Fuels 24 (2010) 5829–5833.
[45] W. Farneth, R. Gorte, Chem. Rev. 95 (1995) 615–635.
[46] C. Emeis, J. Catal. 141 (1993) 347–354.
[47] A.B. Kellicutt, R. Salary, O.A. Abdelrahman, J.Q. Bond, Catal. Sci. Technol. 4 (2014) 2267–2279.
[48] J.Q. Bond, C.S. Jungong, A. Chatzidimitriou, J. Catal. 344 (2016) 640–656.
[49] O.A. Abdelrahman, A. Heyden, J.Q. Bond, ACS Catal. 4 (4) (2014) 1171–1181.
[50] A. Chatzidimitriou, J.Q. Bond, Green Chem. 17 (8) (2015) 4367–4376.
[51] J. Liu, R. Lin, Y. Nan, L.L. Tavlarides, J. Supercrit. Fluids 99 (2015) 38–50.
[52] Reference Fluid Thermodynamic and Transport Properties, NIST Standard Reference Database 23, Version 9.0. National Institute of Standards and Technology, Boulder, CO, 2018, p. 80305.
[53] Standard Test Method for Determination of Total Monoglycerides, Total Diglycerides, Total Triglycerides, and Free and Total Glycerin in B-100 Biodiesel Methyl Esters by Gas Chromatography, ASTM International, West Conshohocken, PA, 2012.
[54] M.G. Kulkarni, R. Gopinath, L.C. Meher, A.K. Dalai, Green Chem. 8 (2006) 1056–1062.
[55] M.R. Gafurov, I.N. Mukhambetov, B.V. Yavkin, G.V. Mamin, A.A. Lamberov, S.B. Orlinskii, J. Phys. Chem. C. 49 (2015) 27410–27415.
[56] H. Xiong, H.N. Pham, A.K. Datye, Green Chem. 16 (2014) 4627–4643.